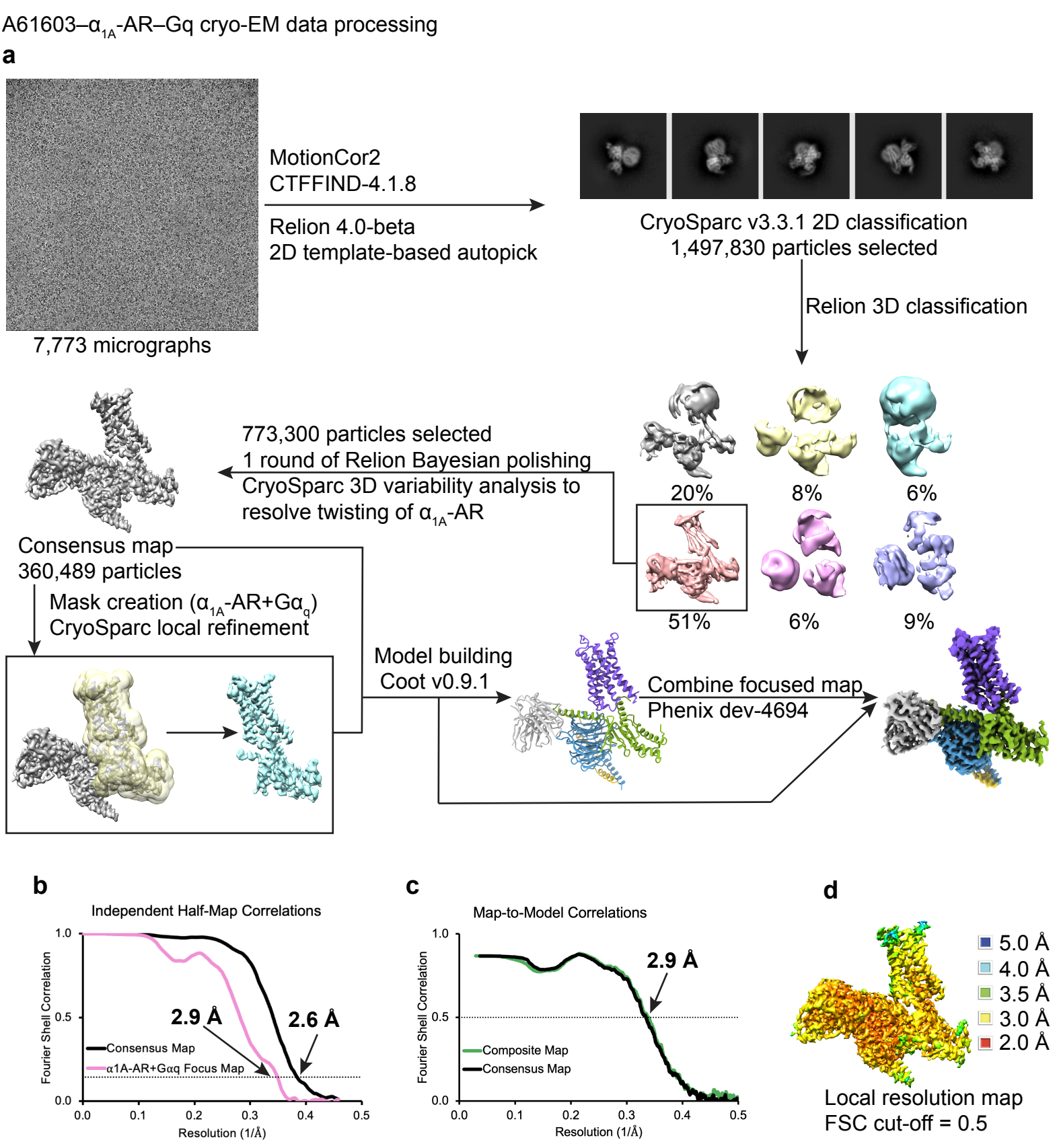


**Supplementary Figure 1. A61603–$\alpha_{1A}$-AR–Gq cryo-EM data processing.**
**a,** Cryo-EM data processing workflow of A61603–$\alpha_{1A}$-AR–Gq complex. **b**, Fourier shell correction curves of consensus map and $\alpha_{1A}$-AR and G$\alpha_q$ focus map. **c**, Cross-validation of consensus and composite maps to A61603–$\alpha_{1A}$-AR–Gq complex model. **d**, Local resolution of consensus map.

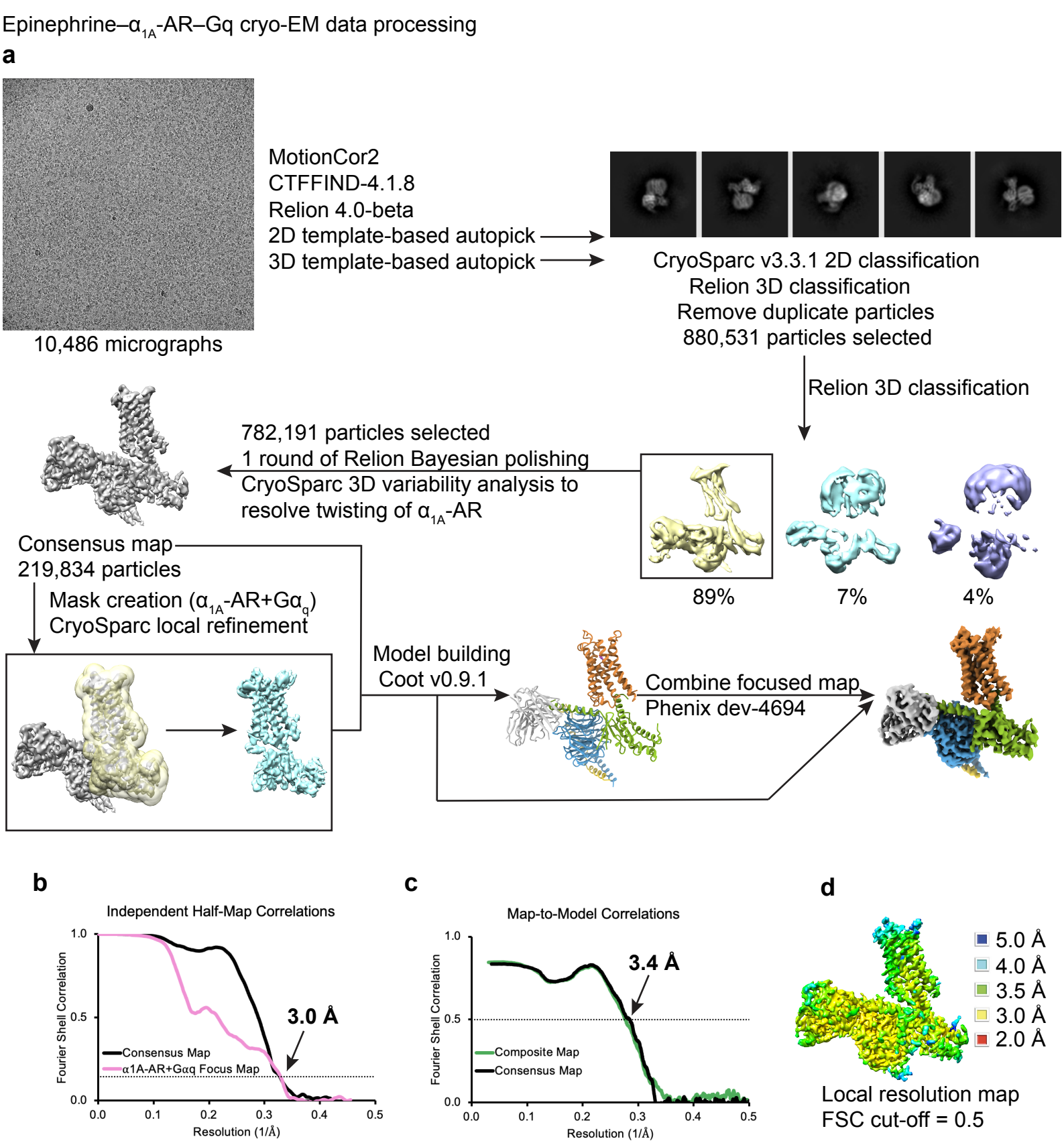


**Supplementary Figure 2. Epinephrine–$\alpha_{1A}$-AR–Gq cryo-EM data processing.**
**a,** Cryo-EM data processing workflow of epinephrine–$\alpha_{1A}$-AR–Gq complex. **b**, Fourier shell correction curves of consensus map and $\alpha_{1A}$-AR and $G\alpha_q$ focus map. **c**, Cross-validation of consensus and composite maps to epinephrine–$\alpha_{1A}$-AR–Gq complex model. **d**, Local resolution of consensus map.

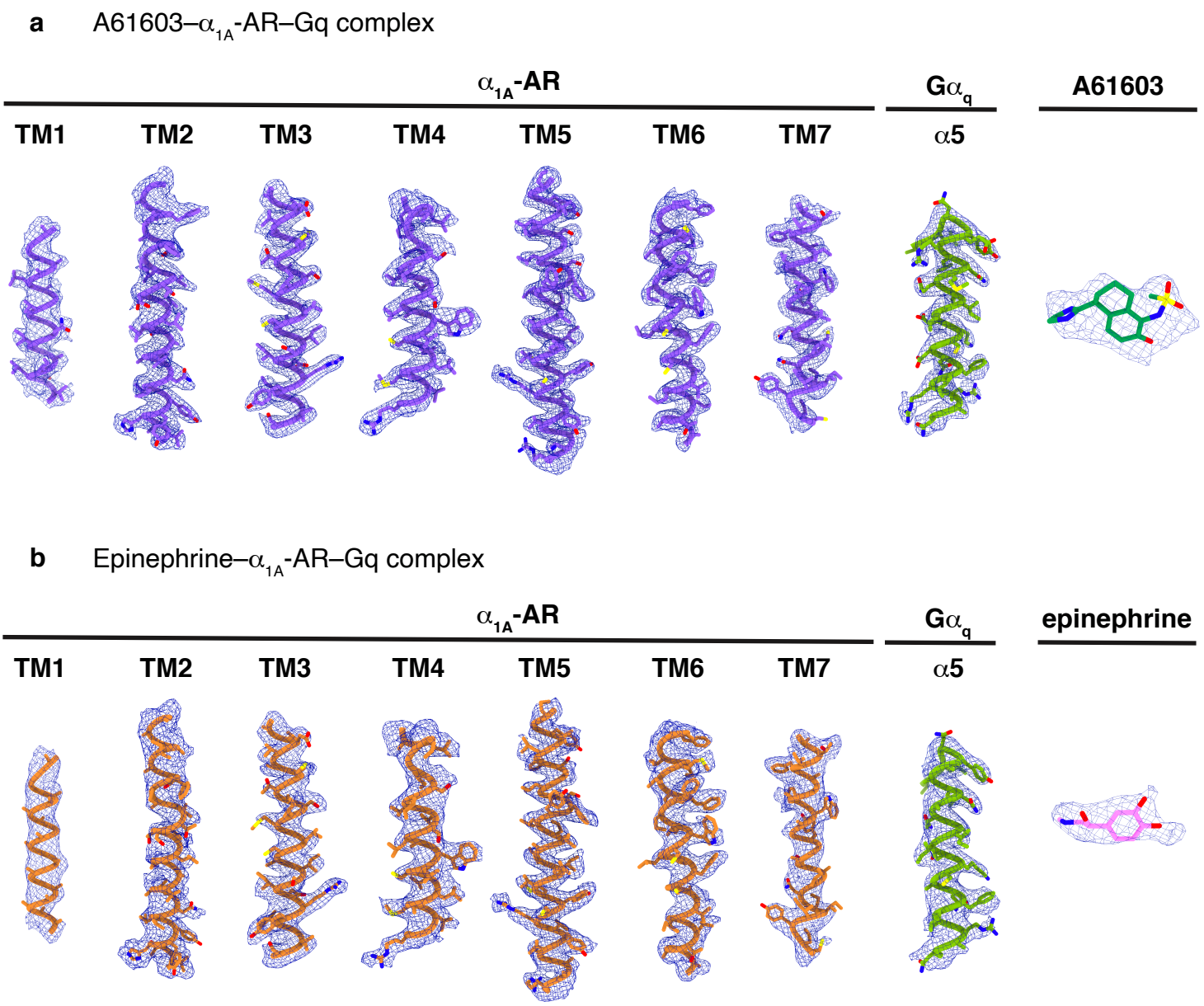


**Supplementary Figure 3. Cryo-EM maps versus refined structures.**
Cryo-EM density maps and models are shown for all seven transmembrane α-helices of $\alpha_{1A}$-AR and α5-helix of $G\alpha_q$, of A61603–$\alpha_{1A}$-AR–$G_q$ complex **(a)** and epinephrine–$\alpha_{1A}$-AR–$G_q$ complex **(b)**.

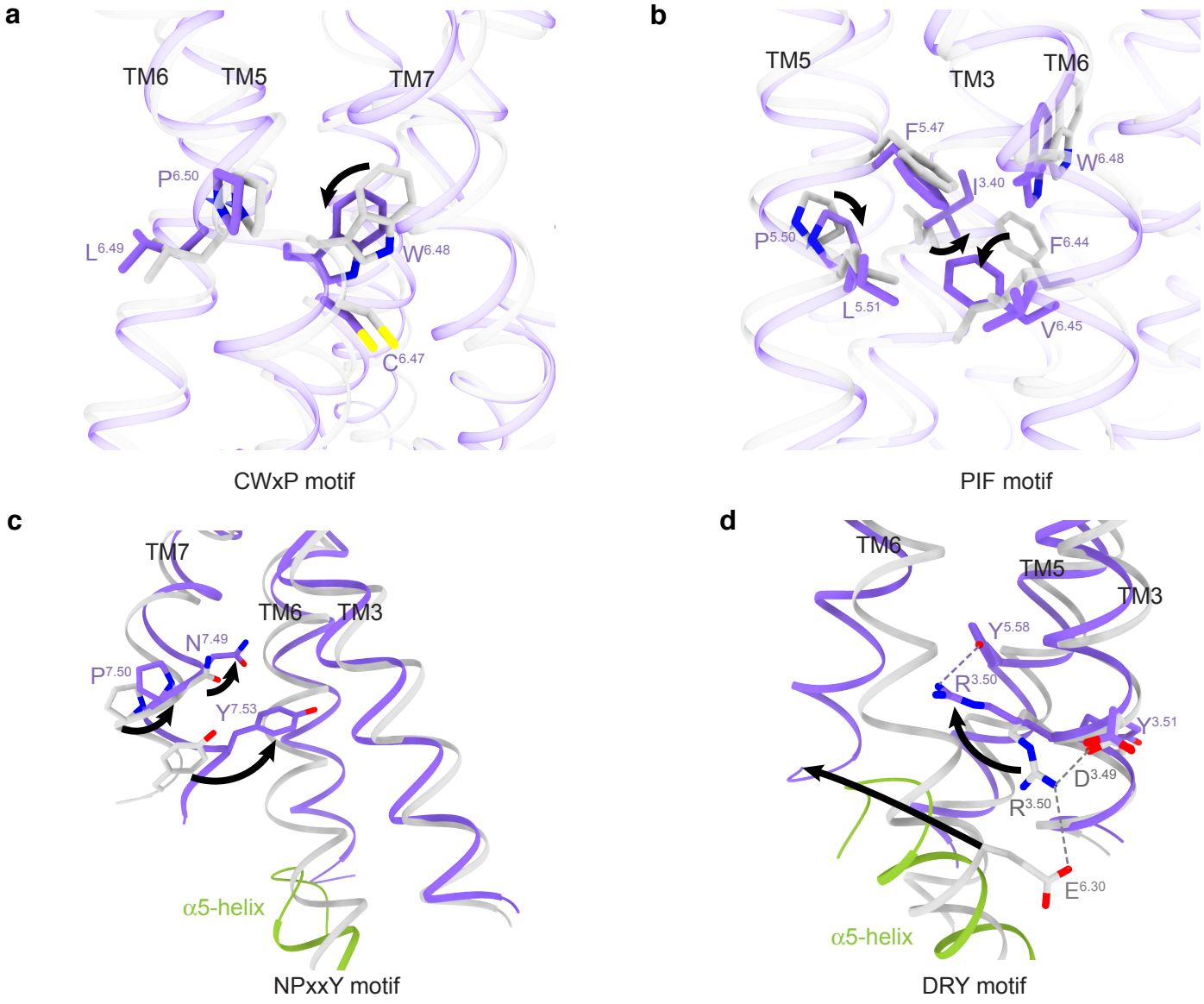


**Supplementary Figure 4. Conformational changes of $\alpha_1$-AR during the activation.**
Structural comparisons of the inactive state $\alpha_{1B}$-AR (grey; PDB 7B6W) and the active state of $\alpha_{1A}$-AR in complex with Gq (this work) are shown. (**a**) The conformational changes of the CWxP motif during $\alpha_1$-AR activation are shown. (**b**) The conformational changes of the PIF motif during $\alpha_1$-AR activation are shown. (**c**) Movement of $Y^{7.53}$ within the NPxxY motif. (**d**) The conformational changes in the DRY motif.

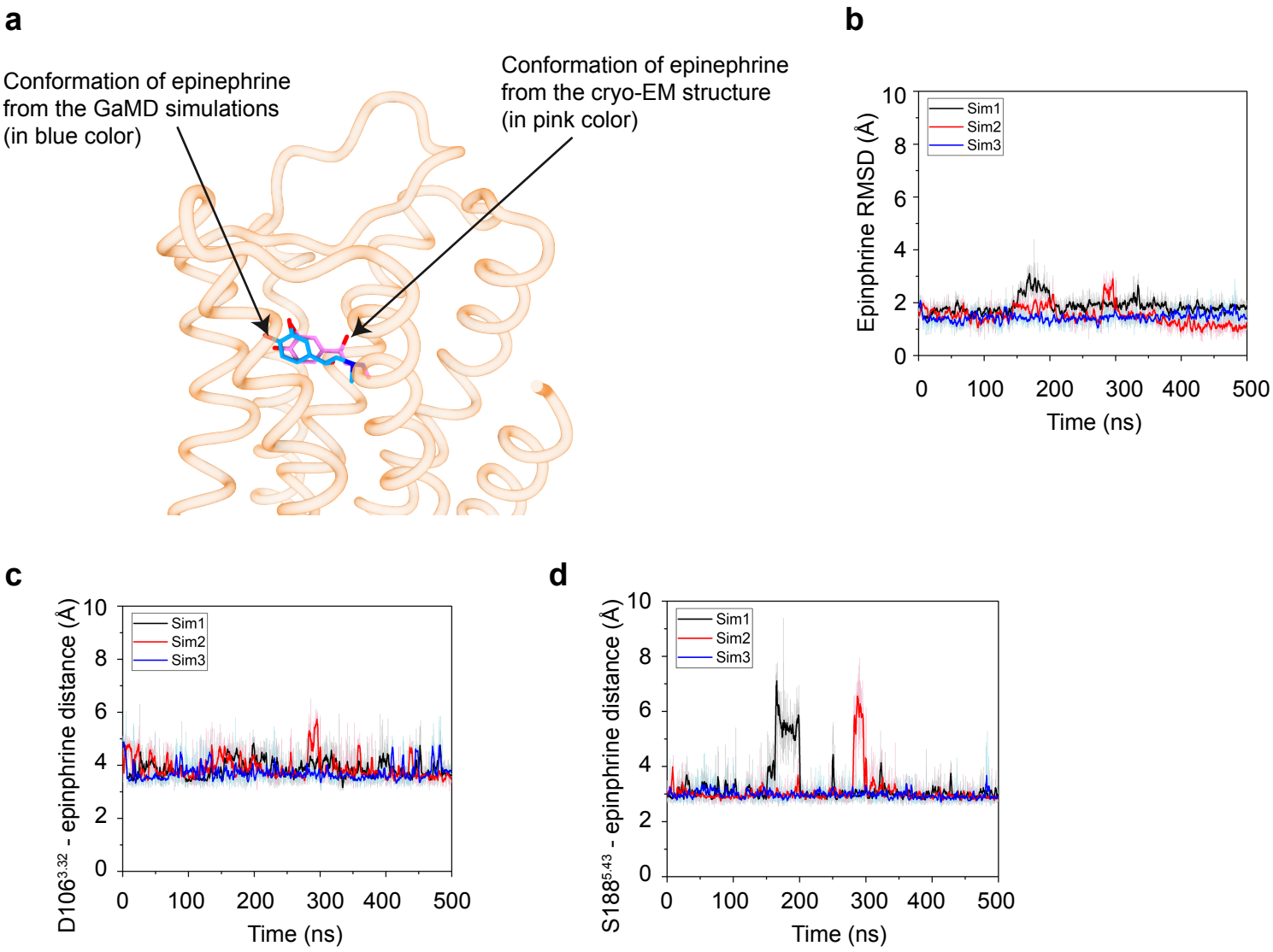


**Supplementary Figure 5**. **GaMD simulations of epinephrine.**
(**a**) Comparison of the conformations of epinephrine in the cryo-EM structure (in pink color) and from GaMD simulations (in blue color). (**b**) The epinephrine RMSD by comparing the conformations of epinephrine in the cryo-EM structure and from GaMD simulations. (**c,d**) time courses of the distances between epinephrine and specific residues of $\alpha_{1A}$-AR were calculated from the GaMD simulations: between the CG atom of D106$^{3.32}$ and N1 atom of epinephrine (**c**), and between the OG atom of S188$^{5.43}$ and O2 atom of epinephrine (**d**). Three independent 500 ns GaMD simulations are shown for each condition.

**a. Complex of epinephrine–$\beta_1$-AR–nanobody 6B9**

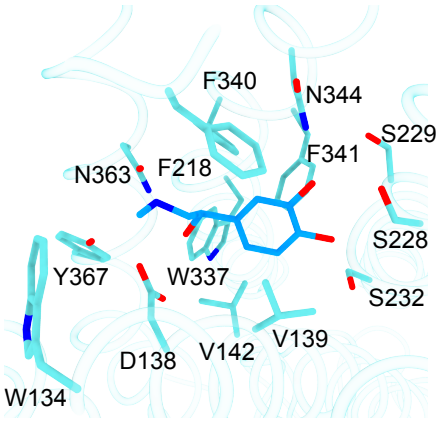


**b. Comparison of epinephrine in complex with $\alpha_{1A}$-AR and with $\beta_1$-AR**

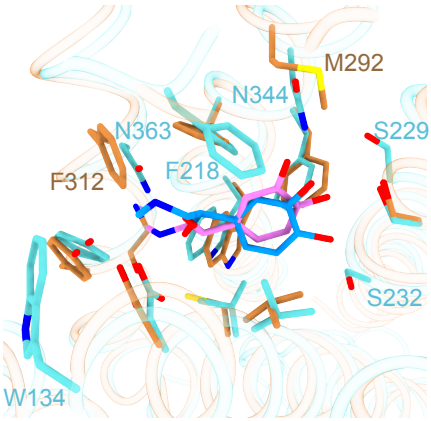


**c. Complex of epinephrine–$\beta_2$-AR–nanobody 6B9**

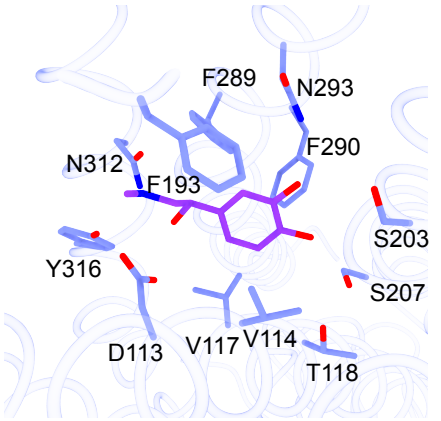


**d. Comparison of epinephrine in complex with $\alpha_{1A}$-AR and with $\beta_2$-AR**

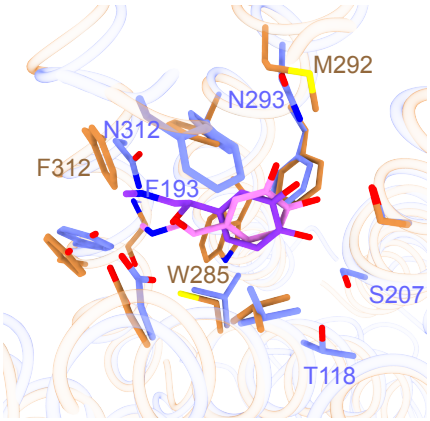


**Supplementary Figure 6. Different conformations of epinephrine.**
**(a)** epinephrine in the complex of epinephrine–$\beta_1$-AR–nanobody 6B9. **(b)** Comparison of epinephrine in complex with $\alpha_{1A}$-AR and with $\beta_1$-AR. (**c**) Epinephrine in the complex of epinephrine–$\beta_2$-AR–nanobody 6B9. (**d**) Comparison of epinephrine in complex with $\alpha_{1A}$-AR and with $\beta_2$-AR.

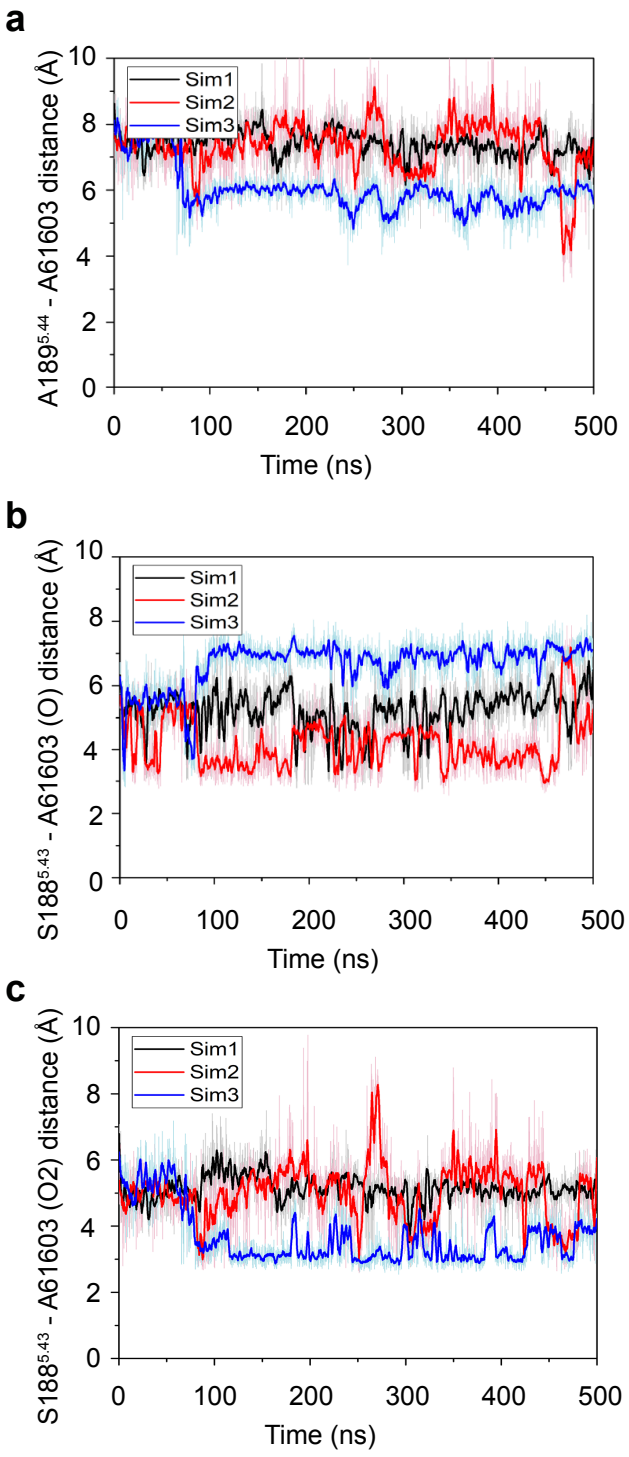


**Supplementary Figure 7**. **GaMD simulations of A61603.**
Time courses of the distances between A61603 and specific residues of $\alpha_{1A}$-AR were calculated from the GaMD simulations: the N atom of A189$^{5.44}$ and the O2 atom of A61603 (**a**), the OG atom of S188$^{5.43}$ and the O atom of A61603 (**b**), and the OG atom of S188$^{5.43}$ and the O2 atom of A61603 (**c**). Three independent 500 ns GaMD simulations are shown for each condition.

**a. Phylogenetic tree of all human ARs**

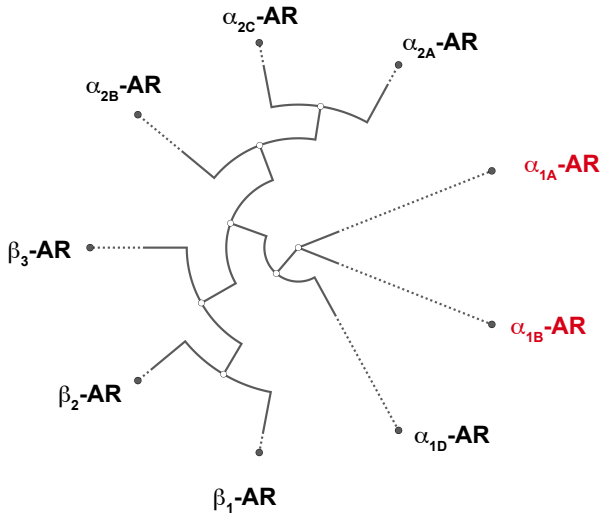


**b. Most of A61603 interacting residues are conserved in $\alpha_1$-ARs**

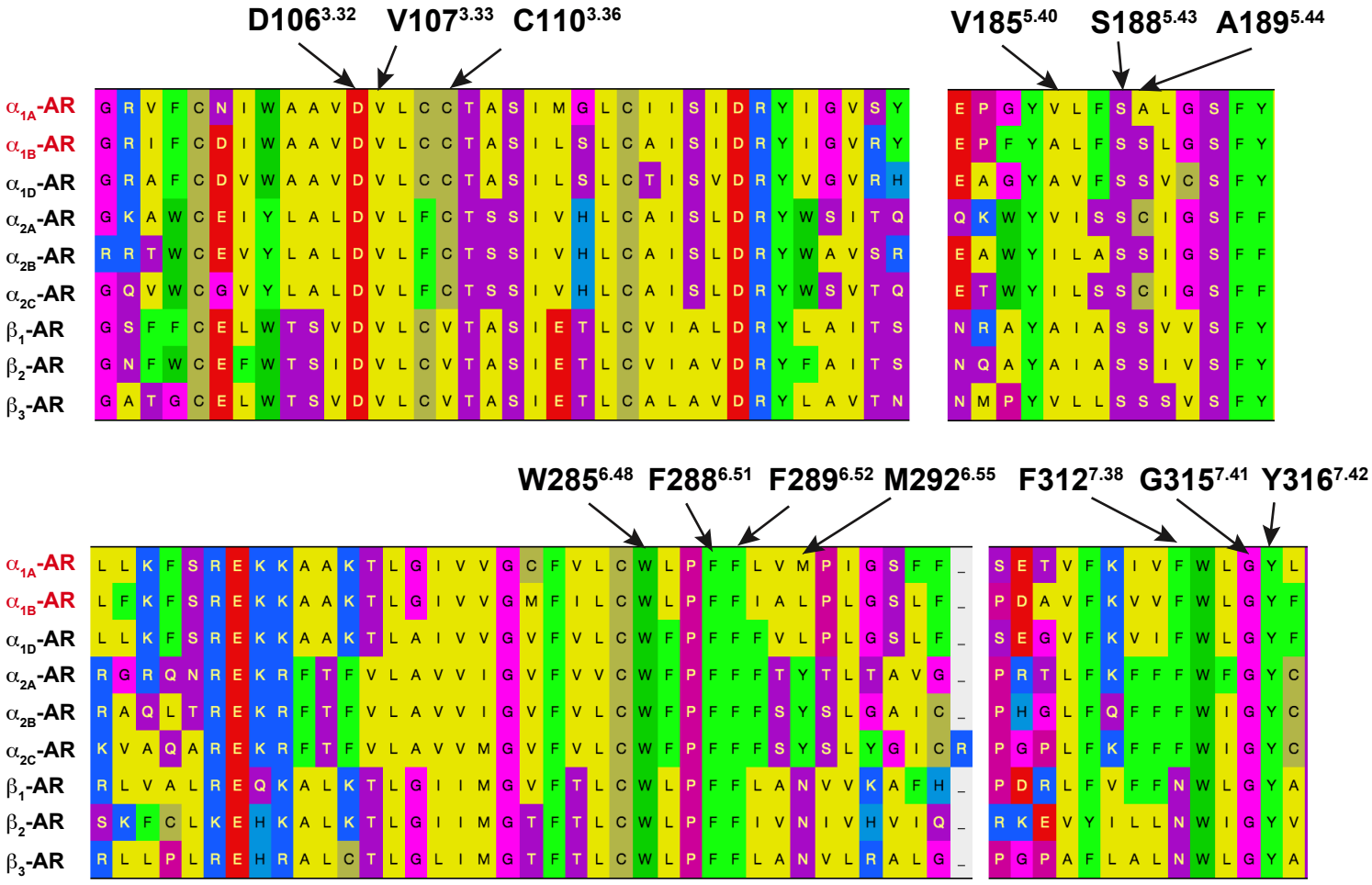


**Supplementary Figure 8. Conservation assessments of all human ARs.**
**(a)** Phylogenetic tree of all human ARs. **(b)** Structure-based sequence alignment of all human ARs generated in GPCRdb. A61603 interacting residues are labeled. As the sequence alignment indicated, most of A61603 interacting residues are conserved in $\alpha_1$-ARs.

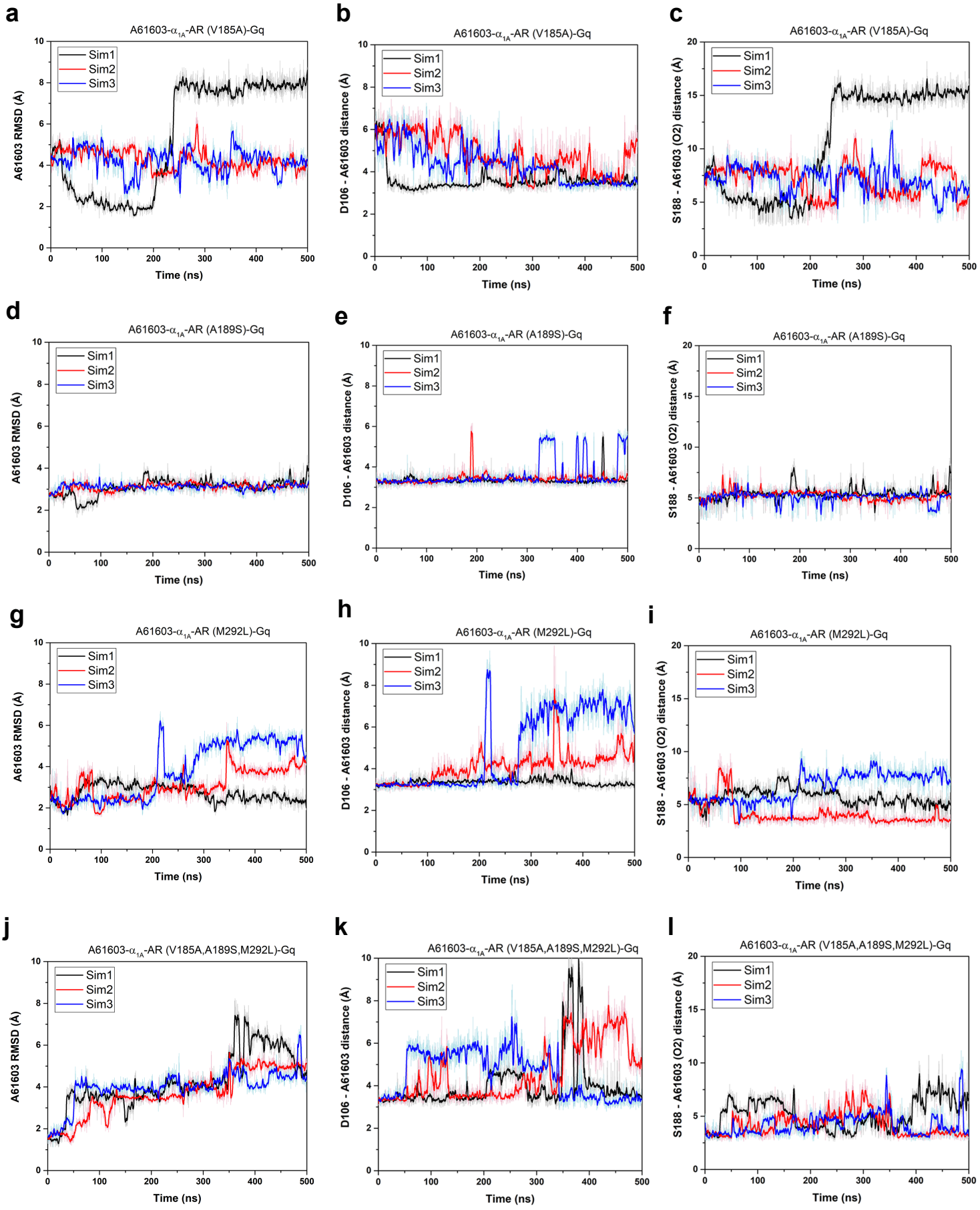


**Supplementary Figure 9**. **GaMD simulations of A61603 in complexes with mutant $\alpha_{1A}$-ARs.** Time courses of A61603 RMSDs relative to the initial structures in the systems of $\alpha_{1A}$-AR(V185A) (**a-c**), $\alpha_{1A}$-AR(A189S) (**d-f**), $\alpha_{1A}$-AR(M292L) (**g-i**), and $\alpha_{1A}$-AR(V185A,A189S,M292L) (**j-l**). Time courses of the distances between A61603 and specific residues of mutant $\alpha_{1A}$-ARs were calculated from the GaMD simulations: the CG atom of D106$^{3.32}$ and the N2 atom of A61603 (**b,e,h,k**), and the OG atom of S188$^{5.43}$ and the O2 atom of A61603 (**c,f,i,l**). Three independent 500 ns GaMD simulations are shown for each condition.

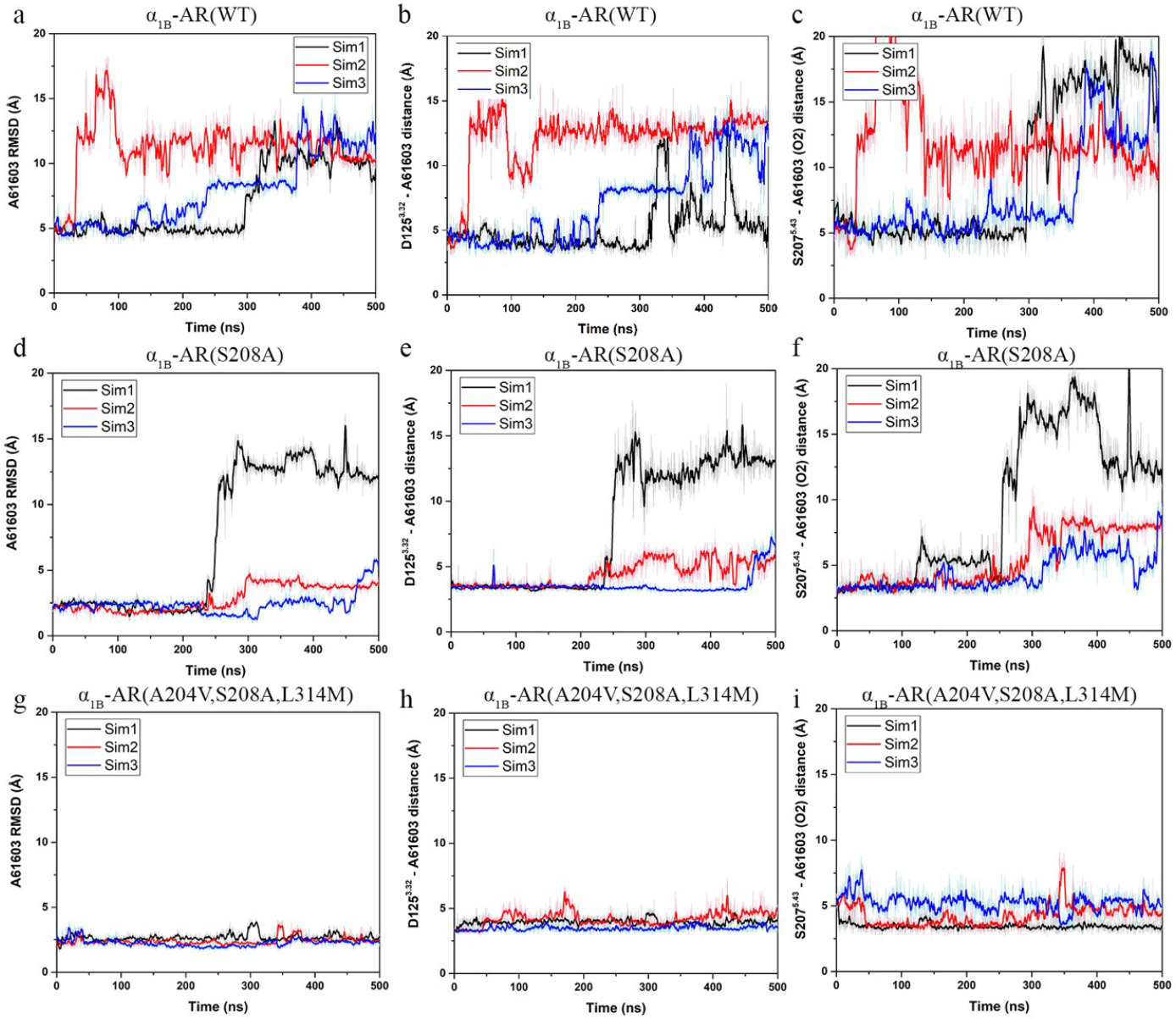


**Supplementary Figure 10**. **GaMD simulations of A61603 in complexes with wild-type and mutant $\alpha_{1B}$-ARs.** (**a, d, g**) Time courses of A61603 RMSDs relative to the initial structures in the system of wild-type $\alpha_{1B}$-AR (**a**), $\alpha_{1B}$-AR(S208A) (**d**) and $\alpha_{1B}$-AR(A204V,S208A,L314M) (**g**). (**b, e, h**) Time courses of the distance between the CG atom of $D125^{3.32}$ and N2 atom of A61603 in the system of wild-type $\alpha_{1B}$-AR (**b**), $\alpha_{1B}$-AR(S208A) (**e**) and $\alpha_{1B}$-AR(A204V,S208A,L314M) (**h**). (**c, f, i**) Time courses of the distance between the OG atom of $S207^{5.43}$ and the O2 atom of A61603 in the wild-type of $\alpha_{1B}$-AR (**c**), $\alpha_{1B}$-AR(S208A) (**f**) and $\alpha_{1B}$-AR (A204V,S208A,L314M) (**i**). Three independent 500 ns GaMD simulations are shown for each condition.

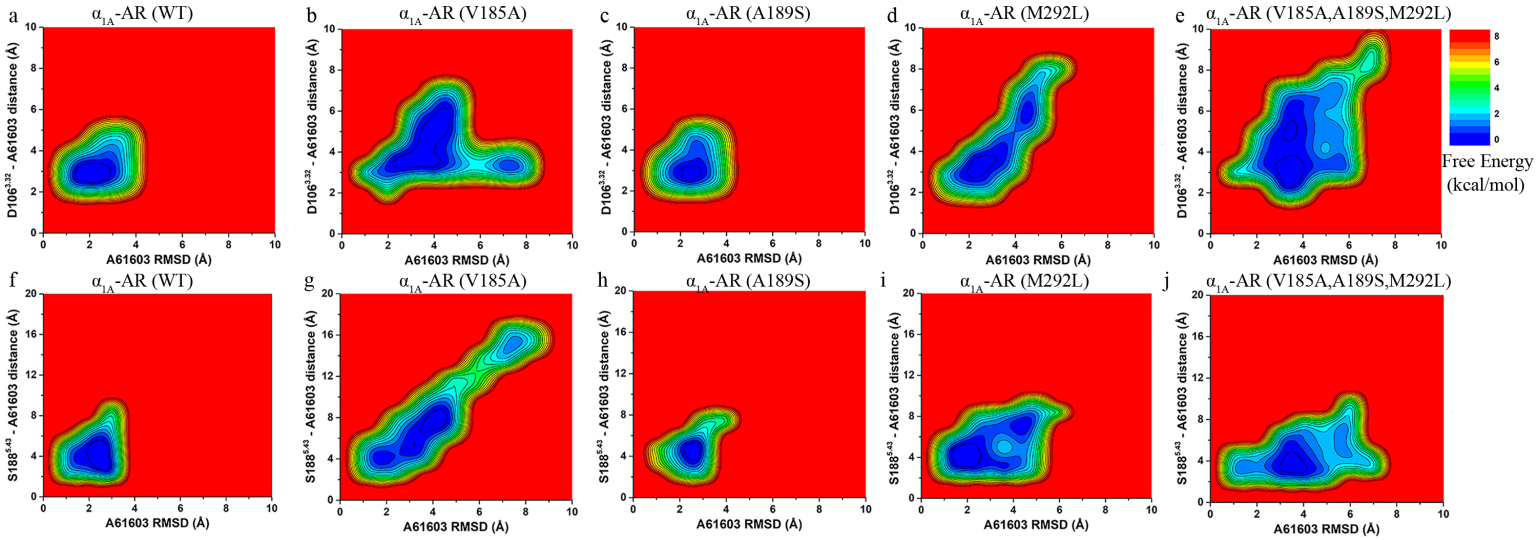


**Supplementary Figure 11**. **2D free energy profiles**.
(**a-e**) 2D free energy profiles of the A61603 RMSD relative to the distance between the CG atom of $D106^{3.32}$ and N2 atom of A61603 in the system of $\alpha_{1A}$-AR (WT) (**a**), $\alpha_{1A}$-AR (V185A) (**b**), $\alpha_{1A}$-AR(A189S) (**c**), $\alpha_{1A}$-AR(M292L) (**d**) and α1A-AR(V185A,A189S,M292L) (**e**). (**f-j**) 2D free energy profiles of the A61603 RMSD relative to the distance between the OG atom of $S188^{5.43}$ and O2 atom of A61603 in the system of $\alpha_{1A}$-AR (WT) (**f**), $\alpha_{1A}$-AR (V185A) (**g**), $\alpha_{1A}$-AR(A189S) (**h**), $\alpha_{1A}$-AR(M292L) (**i**) and α 1A-AR(V185A,A189S,M292L) (**j**).

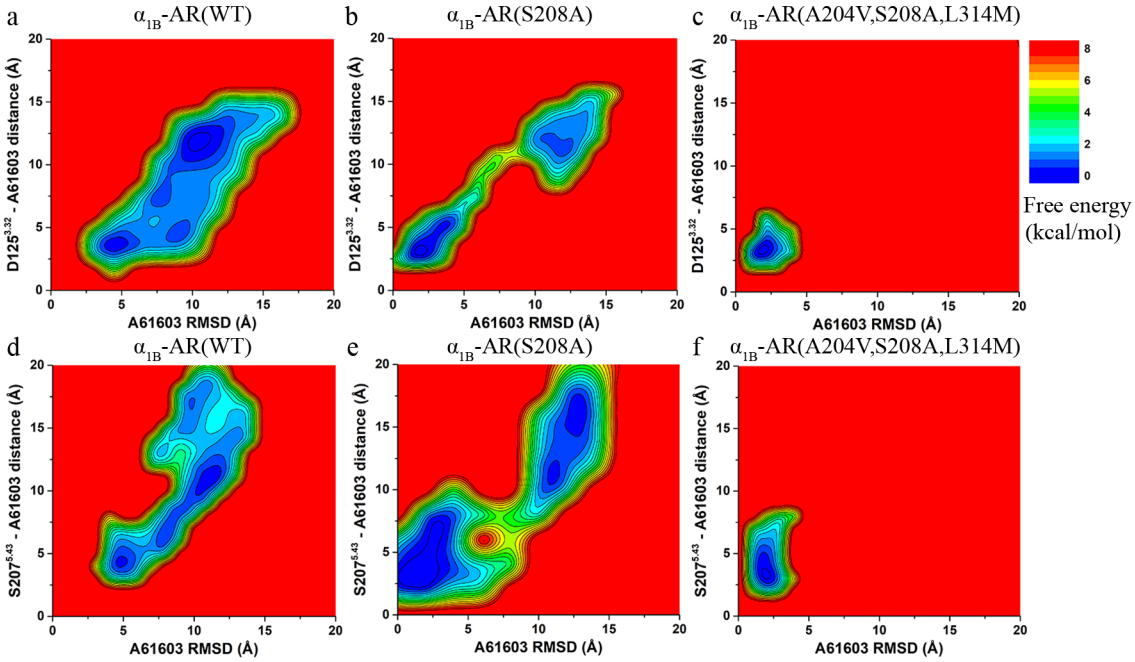


**Supplementary Figure 12**. **2D free energy profiles**.
(**a-c**) 2D free energy profiles of the A61603 RMSD relative to the distance between the CG atom of $D125^{3.32}$ and N2 atom of A61603 in the system of $\alpha_{1B}$-AR (WT) (**a**), $\alpha_{1B}$-AR (S208A) (**b**), and $\alpha_{1B}$-AR(A204V,S208A,L314M) (**c**). (**d-f**) 2D free energy profiles of the A61603 RMSD relative to the distance between the OG atom of $S207^{5.43}$ and O2 atom of A61603 in the system of $\alpha_{1B}$-AR (WT) (**d**), $\alpha_{1B}$-AR (S208A) (**e**), and $\alpha_{1B}$-AR(A204V,S208A,L314M) (**f**).

**Comparison of A61603 and epinephrine conformations and orientations in the complexes with $\alpha_{1A}$-AR and Gq**

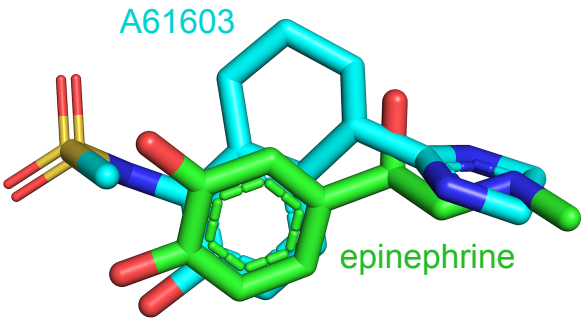


**Supplementary Figure 13. Orientations of A61603 and epinephrine in the complex structures.**
The conformations of A61603 and epinepherine in the cryo-EM structures are compared.

## Supplementary Table 1. Cryo-EM data collection, refinement and validation statistics

| | **A61603–$\alpha_{1A}$-AR–Gq** (EMDB-41267) (PDB 8THK) | **Epinephrine–$\alpha_{1A}$-AR–Gq** (EMDB-41268) (PDB 8THL) |
|---|---|---|
| **Data collection and processing** | | |
| Magnification | 81,000x | 64,000x |
| Voltage (kV) | 300 | 300 |
| Electron exposure ($e^{-}$/Å$^2$) | 50 | 52 |
| Defocus range (μm) | -1.0 to -1.8 | -1.0 to -1.8 |
| Pixel size (Å) | 1.07 | 1.076 |
| Symmetry imposed | C1 | C1 |
| Initial particle images (no.) | 1,497,830 | 880,531 |
| Final particle images (no.) | 360,489 | 219,834 |
| Map resolution (Å) (Full/$\alpha_{1A}$-AR–G$\alpha$ focus) | 2.62/2.86 | 3.07/3.04 |
| FSC threshold | 0.143 | 0.143 |
| **Refinement** | | |
| Initial model used (PDB/ AlphaFoldDB code) | 6WHA and AF-P35348-F1 | 6WHA and AF-P35348-F1 |
| Model resolution (Å) | 2.9/2.4 | 3.4/3.0 |
| FSC threshold | 0.50 / 0.143 | 0.50 / 0.143 |
| Map sharpening *B* factor (Å$^2$) | -50 | -30 |
| Model composition | | |
| Non-hydrogen atoms | 8,159 | 7,837 |
| Protein residues | 1,080 | 1,080 |
| Ligands | 1 | 1 |
| *B* factors (Å$^2$) | | |
| Protein | 57.64 | 105.68 |
| Ligand | 48.76 | 123.23 |
| R.m.s. deviations | | |
| Bond lengths (Å) | 0.002 | 0.003 |
| Bond angles (°) | 0.478 | 0.483 |
| Validation | | |
| MolProbity score | 1.19 | 1.46 |
| Clashscore | 4.00 | 5.70 |
| Poor rotamers (%) | 0.95 | 0.79 |
| Ramachandran plot | | |
| Favored (%) | 98.21 | 97.17 |
| Allowed (%) | 1.79 | 2.83 |
| Disallowed (%) | 0.00 | 0 |

**Supplementary Table 2. Summary of the A61603 root-mean-square-fluctuation (RMSF) and binding free energy from MM/GBSA calculations on wild-type and mutant $\alpha_{1A}$-ARs and $\alpha_{1B}$-ARs. For each system, 1,000 frames were used for MM/GBSA calculations. Mean ± SD are shown.**

| $\alpha_{1A}$-AR | | | | | |
|---|---|---|---|---|---|
| System | WT | V185A | A189S | M292L | V185A,A189S,M292L |
| A61603 RMSF (Å) | 1.46 ± 0.10 | 2.36 ± 0.52 | 1.10 ± 0.09 | 1.74 ± 0.39 | 2.58 ± 0.33 |
| A61603 binding free energy (kcal/mol) | -26.73 ± 0.22 | -22.18 ± 0.73 | -26.54 ± 1.89 | -27.88 ± 1.53 | -11.52 ± 2.47 |
| $\alpha_{1B}$-AR | | | | | |
| System | WT | S208A | A204V,S208A,L314M | | |
| A61603 RMSF (Å) | 4.28 ± 0.30 | 3.55 ± 1.97 | 0.98 ± 0.21 | | |
| A61603 binding free energy (kcal/mol) | -11.52 ± 2.47 | -25.81 ± 2.67 | -28.21 ± 2.80 | | |